Computer Physics Communications 183 (2012) 1237–1245

Contents lists available at SciVerse ScienceDirect

Computer Physics Communications

www.elsevier.com/locate/cpc

Reverse Monte Carlo modeling of thermal disorder in crystalline materials from EXAFS spectra

Janis Timoshenko *, Alexei Kuzmin, Juris Purans

Institute of Solid State Physics, University of Latvia, Kengaraga street 8, LV-1063 Riga, Latvia

ARTICLE INFO

Article history:
Received 31 August 2011
Received in revised form 16 January 2012
Accepted 2 February 2012
Available online 6 February 2012

Keywords:
Reverse Monte Carlo
EXAFS
Wavelet analysis
Germanium
Rhenium trioxide

ABSTRACT

In this work we present the Reverse Monte Carlo (RMC) modeling scheme, designed to probe the local structural and thermal disorder in crystalline materials by fitting the wavelet transform (WT) of the EXAFS signal. Application of the method to the analysis of the Ge K-edge and Re L_3-edge EXAFS signals in crystalline germanium and rhenium trioxide, respectively, is presented with special attention to the problem of thermal disorder and related phenomena.

1. Introduction

Reverse Monte Carlo (RMC) method is a simulation technique, which allows one to determine a 3D model of the material atomic structure by minimizing the difference between its structure-related experimental and calculated properties [1]. The method does not require knowledge of interatomic potentials that is its main advantage over such simulation techniques as conventional Monte Carlo or molecular dynamics (MD). However, such information can be utilized to exclude unphysical solutions as has been recently demonstrated in the hybrid RMC method [2].

Practical application of the RMC method relies on the high computing speed, since the involved structural models are usually large, the calculation of properties can be computationally heavy, and the minimization algorithm, based on the random (i.e., Monte Carlo) process, requires very many steps till it converges to a solution. Therefore, the popularity of the RMC method during the last two decades [3,4] is driven by the wide spread occurrence of high-performance computing systems.

Original use of the RMC method [1] and most of its recent applications [3,5] concern with the reconstruction of the atomic structure in the disordered materials (glasses and liquids) from the diffraction (neutron, X-ray, electron) data. However, the application of the method to crystalline [6–10] and nanocrystalline [11–14] compounds is also useful to study deviations from the average atomic structure due to the presence of thermal disorder or local structural distortions.

The application of the RMC method to the analysis of the extended X-ray absorption fine structure data (EXAFS) has been addressed in a number of works [15–26]. Most previous EXAFS studies have been based on the single-scattering approximation formalism, thus accounting only for the contribution of pair-distribution functions, that limits accurate analysis to the first coordination shell around the absorber. At the same time, the sensitivity of EXAFS to higher-order distribution functions through the multiple-scattering (MS) contributions has been discovered as early as in 1975 in metallic copper [27,28]. It was demonstrated in [27,28] that the amplitude of scattered photoelectron wave is strongly affected in nearly collinear atomic chains, thus leading to an increase of the EXAFS signal amplitude from outer coordination shells. This phenomenon, known as the "focusing" effect, has been later found and interpreted in many materials, for example, having perovskite-type structure such as ReO_3 [29–31], $NaWO_3$ [32], WO_{3-x} [33], and FeF_3 [34]. Note that the accurate description of the "focusing" effect in perovskites allows the quantitative estimation of the bonding angles between structural units, in this case, the coordination octahedra, which are strictly connected to the physical properties of the materials [35]. Besides the outer shell MS contributions, the MS signals generated within the first coordination shell of the absorber can be also important: their contribution depends strongly on the path geometry, i.e., structural units distortion, and the atoms involved in the scattering process [36]. Such MS processes contribute between the peaks of the first and second coordination shells in the Fourier transform of the EXAFS spectra and are easily observed in the case of the octahedral absorber coordination as in perovskites [31,32] or ions of 3*d*-transition metals in solutions [37,38].

* Corresponding author.
E-mail address: timoshenkojanis@inbox.lv (J. Timoshenko).

0010-4655/$ – see front matter
doi:10.1016/j.cpc.2012.02.002

Nowadays it becomes a challenging task to extract the information on the higher-order distribution functions from the total EXAFS signal. The possibility to solve such problem has been demonstrated by Di Cicco et al. [18,19] on the example of liquid copper, where the three-body contribution was clearly identified from the RMC analysis of the Cu K-edge EXAFS $\chi(k)k$ signal in k-space. The extension of this approach to crystalline compounds, having smaller degree of structural and thermal disorder, is heavy computational task, since in the ordered materials the number of multiple-scattering paths increases rapidly upon an increase of the radial distance from the absorber. This problem has been addressed recently within two computer codes – the RMCProfile code [39] and the SpecSwap-RMC code [25]. In the method by Krayzman et al. [24,26], implemented as an extension to the RMCProfile code [39], the calculation of the double- and triple-scattering events is included in the RMC-EXAFS analysis in approximative way by evaluating the scattering amplitudes and phase shifts for each path prior to refinements using the average-configuration model. Another approach is realized within the SpecSwap-RMC code [25]. In this case, the configuration space is reduced and is expressed in terms of a discrete set of local structures, for which the EXAFS signals are pre-computed in advance to decrease significantly the RMC computation time [25].

The RMC modeling scheme, presented in this paper, is primarily designed but not limited to determine the local structural and thermal disorder in crystalline materials from the analysis of the experimental EXAFS signal within the multiple-scattering formalism. Unlike previous works, our RMC algorithm is able to minimize the difference between experimental and calculated EXAFS signals not only in the energy (k) or real (R) space independently, but also simultaneously by comparing their wavelet transforms [40]. Besides, we use slowly reducing "temperature" parameter in the Metropolis algorithm during the simulations to improve convergence (the so-called simulated annealing method [41]). Since the RMC scheme can be efficiently parallelized, it has been implemented on the high-performance computing (HPC) cluster at the Institute of Solid State Physics (Riga) [42], thus allowing one to solve a typical task within a few days of computational time.

The paper is organized in the four main sections. In Section 2 our RMC simulation scheme is described in details. In Section 3 the application of the RMC method is illustrated on the example of model configuration-averaged EXAFS signal, calculated from the results of the MD simulations [43]. Such approach allows us to validate just the RMC algorithm, thus excluding possible problems related to the accuracy of the EXAFS signal calculation. In Section 4 the RMC method is applied to the analysis of the experimental data: Ge K-edge in crystalline germanium (Ge) [44] and Re L_3-edge [45] EXAFS signals in crystalline rhenium trioxide (ReO_3).

2. RMC-EXAFS modeling scheme

2.1. Calculation of the EXAFS signal

The RMC procedure requires at each step to calculate the total EXAFS signal $\chi_{\mathrm{tot}}(k)$, corresponding to the current atomic configuration, to be compared with the experimental one $\chi_{\mathrm{exp}}(k)$. The total EXAFS signal $\chi_{\mathrm{tot}}(k)$ equals to the average of the EXAFS signals $\chi(k)$ for all absorbing atoms of the same type in the atomic configuration. These signals can be calculated by one of the ab initio EXAFS codes as, for example, FEFF [46] or GNXAS [47]. In fact, the accuracy of the atomic structure reconstruction by the RMC approach is strongly linked to the accuracy of the EXAFS code and, thus, will be undoubtedly improved in the future following developments within the EXAFS theory [48].

In this work, we use the ab initio self-consistent real space multiple-scattering approach as is implemented in the FEFF8 code [46,49], and the EXAFS signal $\chi(k)$ is described by the equation

$$\chi(k) = S_0^2 \sum_j \frac{|f_j(k, \vec{r}_1, \ldots, \vec{r}_m)|}{kR_j^2} \times \sin\bigl(2kR_j + \phi_j(k, \vec{r}_1, \ldots, \vec{r}_m)\bigr). \quad (1)$$

Here the summation is carried out over all possible scattering paths of the photoelectron up to the eight order, when required. $k = \sqrt{(2m_e/\hbar^2)(E - E_0)}$ is the photoelectron wavenumber (m_e is the electron mass, $\hbar$ is Planck's constant, E is the X-ray photon energy, and E_0 is the photoelectron energy origin ($k = 0$)), S_0^2 is the amplitude reduction factor accounting also for multi-electron processes, and R_j is the half length of the j-path.

The scattering amplitude $f_j(k, \vec{r}_1, \ldots, \vec{r}_m)$ and phase shift $\phi_j(k, \vec{r}_1, \ldots, \vec{r}_m)$ functions describe the interaction of the photoelectron with the atoms along the scattering path. They depend on the photoelectron energy and both radial and angular characteristics of the scattering path ($\vec{r}_i$ is the position of the i-th atom), thus being responsible for the sensitivity of the total EXAFS signal to many-body distribution functions, i.e., 3D atomic structure.

The calculation of the f_j and ϕ_j functions in the FEFF8 code requires the knowledge of the cluster potential. It can be evaluated for the average atomic configuration, thus neglecting the potential variation due to thermal vibrations, or recalculated at each RMC step. In this work, since we deal with the crystalline compounds and only thermal disorder is present, the self-consistent cluster potential was evaluated before the RMC run for the average crystalline structure known from diffraction studies. This allowed us to reduce significantly the total computation time. The self-consistent cluster potential was constructed within the muffin-tin approximation, and the complex exchange-correlation Hedin–Lundqvist potential and default values of muffin-tin radii, as provided within the FEFF8 code [46], were used.

2.2. The RMC scheme

First, we will briefly describe the basic RMC algorithm. More details can be found in [3,4].

The RMC simulation starts with an arbitrary initial configuration of atoms in a cell of chosen size and shape with periodic boundary conditions, for which the total EXAFS signal $\chi_{\mathrm{tot}}(k)$ is calculated as described above in Section 2.1. The number of atoms in the cell should give the atomic number density equal to the experimental value. Note that in the case of crystalline material, the cell is often called as a "supercell", since it can be composed of several unit cells.

Next the current atomic configuration is modified by randomly changing the coordinates of one or all atoms, thus producing the new atomic configuration, for which the total EXAFS signal $\chi_{\mathrm{tot}}^{\mathrm{new}}(k)$ is calculated. The two calculated EXAFS signals $\chi_{\mathrm{tot}}^{\mathrm{old}}(k)$ and $\chi_{\mathrm{tot}}^{\mathrm{new}}(k)$ are compared with the experimental one $\chi_{\mathrm{exp}}(k)$, and the new atomic configuration is either accepted or discarded depending on the results of this comparison. The procedure is repeated as many times as needed till the atoms in the cell will occupy such positions that the sum of weighted squared differences ξ_k between theoretical $\chi_{\mathrm{tot}}(k)$ and experimental $\chi_{\mathrm{exp}}(k)$ EXAFS spectra

$$\xi_k = \frac{\|\chi_{\mathrm{tot}}(k)k^n - \chi_{\mathrm{exp}}(k)k^n\|_2}{\|\chi_{\mathrm{exp}}(k)k^n\|_2} \quad (2)$$

is minimized in k-space. Here $\|\ldots\|_2$ denotes the Euclidean norm, and k^n ($n = 1$, 2, or 3) is the usual EXAFS signal weighting factor. The final atomic configuration gives a 3D structure that is consistent with the experimental EXAFS data. Note that the function

$\chi_{exp}(k)$ can correspond to the full experimental EXAFS signal or to its part, obtained by the Fourier filtering procedure in the required R-space range. In fact, the largest distance R_{max}, which can be included in the analysis, is limited by the number of multiple-scattering paths, which can be treated within the ab initio EXAFS code, and by the computation time. In this work, we used $R_{max} = 6$ Å.

Alternatively, one can calculate the Fourier transforms of the total theoretical and experimental EXAFS signals and perform minimization of their differences in the real space (R-space)

$$\xi_R = \frac{\|FT_{tot}(R) - FT_{exp}(R)\|_2}{\|FT_{exp}(R)\|_2}. \quad (3)$$

Third and, to our knowledge, previously unused possibility is to minimize the difference between theory and experiment in both k and R spaces simultaneously by using the so-called wavelet transform (WT) of the EXAFS signal [40,50]. While different types of the WT are known [50], we use the modified Morlet continuous wavelet transform, described in [40]. In this case, the difference is calculated as

$$\xi_{k,R} = \frac{\|WT_{tot}(k, R) - WT_{exp}(k, R)\|_2}{\|WT_{exp}(k, R)\|_2}, \quad (4)$$

where WT_{tot} and WT_{exp} are the WTs of calculated and experimental EXAFS signals, respectively.

The three methods (Eqs. (2), (3), and (4)) used to estimate the difference between theoretical and experimental EXAFS signals have different sensitivity to their behavior due to the peculiarities of the scattering amplitude f_j and phase shift ϕ_j functions for different elements in the Periodic Table. In particular, the criterion in k-space (Eq. (2)) will better discriminate between heavy and light elements producing stronger contributions into the total EXAFS signal at the large and low k-values, respectively. On the contrary, the criterion in R-space (Eq. (3)) will discriminate contributions by frequencies (i.e., radial distances), and it can be affected by the available EXAFS signal range in k-space and by the choice of the window function used in the Fourier transform. Therefore, we believe that the use of the criterion based on the wavelet transform (Eq. (4)) will provide the best results during minimization since it accounts for the two-dimensional representation of the EXAFS signal with simultaneous localization in energy and frequency space domains [40,50].

Since the lattice parameters of the crystalline material can be determined by diffraction techniques with much higher accuracy (better than 10^{-3} Å), compared to that provided by modern EXAFS analysis (usually about 10^{-2} Å), the RMC simulation of the EXAFS signal for a crystal is performed using a fixed box size, defined by the lattice parameters, and by initial placing of atoms at proper Wyckoff positions. This allows us to account for the information available from diffraction data without the need for the direct simulation of diffraction pattern. However, small random initial displacements for all atoms can be given to include approximately thermal disorder and, thus, to avoid rapid changes of the residual at the beginning of the RMC iteration process. Moreover, the shape of the cell is determined by the crystal symmetry and is not obligatory cubic.

The EXAFS method is sensitive to the local atomic structure (usually up to 10 Å around the absorbing atom) due to the restrictions imposed by the life time of the excitation, including the mean free path of the photoelectron and thermal disorder. Therefore, in a periodic system, one can probe and needs to account for relatively small amount of atoms in a rather small cell, whose size should be at least twice the largest radial distance in the Fourier transform of the EXAFS signal, at which structural contributions are still visible. For example, in the calculations discussed further, the number of atoms is between 100 and 300. To compare, the number of atoms, required for the RMC modeling of disordered materials, is at least 1000 [5].

Once the initial atomic configuration is chosen, one should define the procedure for its modification using random atom displacements. For this purpose at each RMC step, one can either randomly pick one atom and randomly change its coordinates, or can randomly modify coordinates of all atoms. In this work, the latter approach is adopted, and the generation of pseudo-random numbers is performed using the Mersenne–Twister algorithm [51]. Moreover, in the real crystals the displacements of atoms from their equilibrium positions due to thermal vibrations are normally less than few tenths of angstrom. Therefore, in the present work we constrain the displacements of atoms from their equilibrium positions that are known from diffraction experiments to be smaller than 0.2 Å.

2.3. The Metropolis algorithm

Next we will discuss the choice of the "temperature" parameter T in the Metropolis criterion [52] for the acceptance/discarding of the atoms movement.

Let the differences between total calculated and experimental EXAFS signals for the current and new atomic configurations be equal to ξ^{old} and ξ^{new}, respectively. If the new atomic configuration is accepted only for $\xi^{new} < \xi^{old}$ then the difference will always decrease, and after some number of steps it will reach the *local* minimum. In order to ensure that the *global* minimum is found, it is necessary to accept some of the atomic displacements for which $\xi^{new} > \xi^{old}$. Such strategy is realized in the most popular algorithm of the movement acceptance/discarding proposed by Metropolis [52]:

$$\begin{aligned} &\text{if } \xi^{new} < \xi^{old}, \quad \text{the move is accepted,} \\ &\text{if } \xi^{new} > \xi^{old}, \quad \text{the move is accepted, if} \\ &\exp\left(-\left(\xi^{new} - \xi^{old}\right)/T\right) > r, \\ &\quad \text{and discarded otherwise,} \end{aligned} \quad (5)$$

where r is a random number in the range between 0 and 1.

The significant problem is the choice of "temperature" parameter T. If T is too large, the system will reach the global minimum, but will fluctuate around it with large amplitude. If T is too small, the simulation may stuck at some local minimum. The conventional approach (see, for example, in [15]) is to choose T proportional to the noise level of experimental data, so that the value of T is small.

In the simulated annealing approach [41], the parameter T is not fixed but decreases slowly. One starts with large value of T to stimulate a fast approach to the global minimum. Then the parameter T decreases, so that the fluctuations of the system becomes damped. At the end of the simulation, T is equal to 0 and, if the annealing has been carried out slowly enough, the system reaches the global minimum. The efficiency of this approach strongly depends on the so-called "cooling schedule" – the function that controls the decrease of T during the simulation. Note that different cooling schedules should be used for different parameters of the modeled system.

In our RMC scheme, we suggest to determine the cooling schedule automatically using the information about the average changes of the residual during the simulation.

By looking at Eq. (5), one can see that the parameter T is equal to $-(\xi^{new} - \xi^{old})/\ln p$, where p is the probability to accept a move with $\xi^{new} > \xi^{old}$. Let us assume that at the beginning of the simulation $p = 1$, i.e., all proposed moves are accepted, but at the end

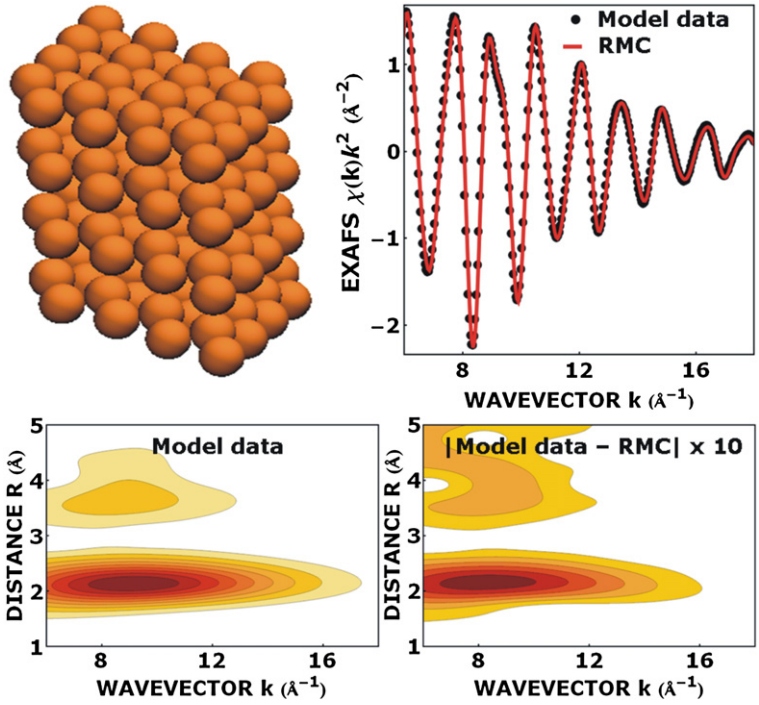

Fig. 1. (Color online.) Upper panel: $4 \times 4 \times 4$ supercell (128 atoms), used in the RMC simulations of crystalline germanium; model Ge K-edge EXAFS signal (dots) and EXAFS signal, obtained in RMC simulations (solid line). Bottom panel: WT moduli for model EXAFS signal and for difference between model and RMC EXAFS signals.

of the simulation $p = 0$, i.e., only the moves with $\xi^{\text{new}} < \xi^{\text{old}}$ are accepted, and in between p changes linearly. By denoting the average change of the difference between theory and experiment per RMC step as Δ and the length of the simulation as $t_{\max}$, one can obtain simple equation for the parameter T as a function of the RMC steps number t

$$T(t) = -\Delta(t)/\ln(1 - t/t_{\max}). \tag{6}$$

The parameter Δ can be obtained by averaging the differences $(\xi^{\text{new}} - \xi^{\text{old}})$ and depends on the system parameters (for example, Δ is smaller for larger number of atoms). During the simulation the parameter Δ changes slowly and can be considered constant.

Following the Hajek theorem [53,54], the simulated annealing algorithm converges if $\sum_{t=1}^{\infty} \exp[-d/T(t)] = \infty$, where d is positive constant that characterize the maximal height of barrier that must be overcome to escape from local minima. In our case, this condition can be rewritten as

$$\lim_{t_{\max}\to\infty} \sum_{t=1}^{t_{\max}} (1 - t/t_{\max})^{d/\Delta} = \infty, \tag{7}$$

and it is satisfied for all values of d and Δ.

3. Application of the RMC-EXAFS method to model data

3.1. The RMC simulation details

To test our RMC scheme, we apply it first to synthetic Ge K-edge EXAFS signal in crystalline germanium (space group $Fd\bar{3}m$). It was calculated using the results of molecular dynamics (MD) simulation, based on the Stillinger–Weber potential (force field) [43] and performed within the NVT ensemble for the lattice constant $a_{\text{Ge}} = 5.658$ Å [55] at the effective temperature of 395 K. It has been shown in [43], that the theoretical EXAFS signal, obtained within such simulation, is very similar to the real Ge K-edge EXAFS spectrum of crystalline germanium at 300 K.

The RMC simulation cell was composed of 64 unit cells of germanium, forming a $4 \times 4 \times 4$ supercell with 128 atoms inside. The total number of the RMC steps was 40 000. The difference ξ_k between calculated by RMC and model EXAFS signals has been calculated in k-space by Eq. (2). The obtained result is shown in Fig. 1, where the supercell, both EXAFS signals and the wavelet transforms of the model EXAFS signal and difference between the model and calculated signals are presented. In Fig. 2 the comparison between the model and calculated signals is separately shown for single-scattering and multiple-scattering contributions. It can be seen, although for the crystalline germanium the changes of EXAFS signal due to the multiple-scattering effects are relatively small, they can be accurately reconstructed and analyzed using our RMC scheme. The time dependencies of the parameters T and ξ_k are shown in Fig. 3.

It should be emphasized that the obtained structural solution, i.e., a set of atomic coordinates, is not unique. Repeating the simulation with the same parameters but with the different sequence of pseudo-random numbers, one will obtain a different set of coordinates. However, the statistical characteristics, such as mean values and dispersions of interatomic distances and bond angles, distribution functions for distances and angles, will be close for both cases, and also close to their "experimental" analogues. This conclusion is supported by the results in Fig. 4, where the radial and angle distribution functions for our MD model are compared with that obtained from RMC simulations: the agreement between both sets of functions for the nearest coordination shells of germanium is very good.

Finally, we compare the values of the mean-square displacements (MSD or $\langle u^2 \rangle$), mean-square relative displacements (MSRD or σ^2) and the mean coordination shell radii $\langle R \rangle$ for the first three coordination shells of Ge in the starting model and as obtained by the RMC simulation (see Table 1). As one can see, our RMC method is able to recover with very good accuracy (less than 1%) the mean shell radii and reasonably well uncorrelated (MSD) and correlated (MSRD) thermal vibration amplitudes.

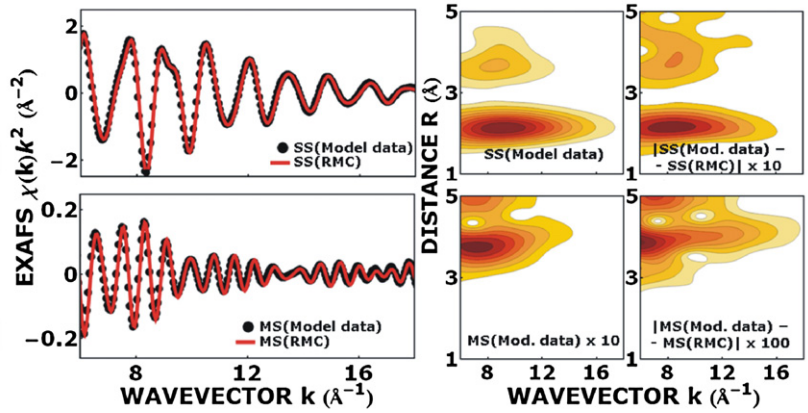

Fig. 2. (Color online.) Model Ge K-edge EXAFS signal (dots) and EXAFS signal, obtained in RMC simulations (solid line) for single-scattering (SS) and multiple-scattering (MS) contributions, WT moduli for corresponding model EXAFS signals and corresponding differences between model and RMC EXAFS signals.

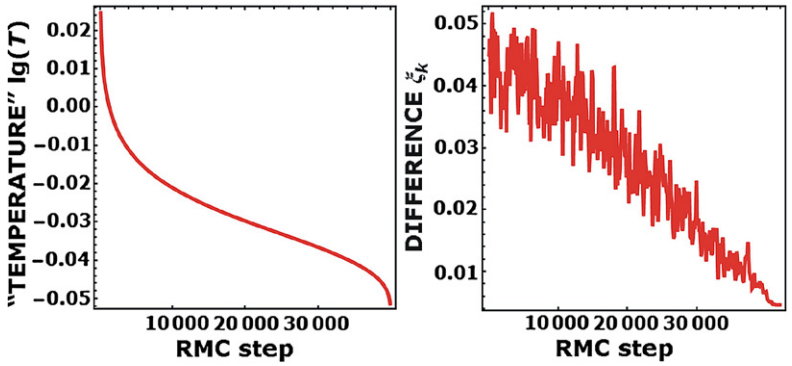

Fig. 3. (Color online.) Dependence of the parameter T and the difference ξ_k on the number of the RMC steps.

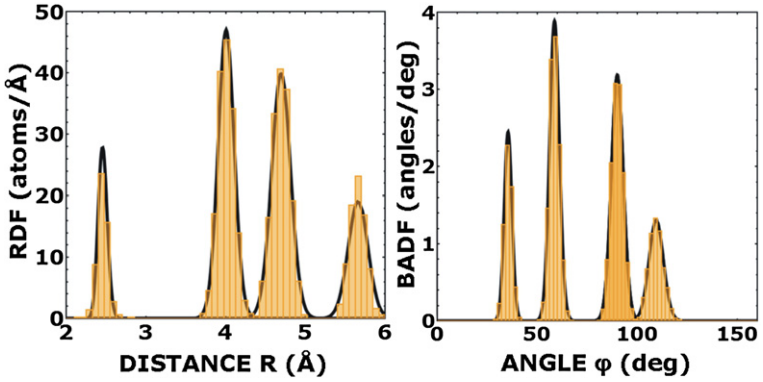

Fig. 4. (Color online.) The radial distribution function RDF (Ge–Ge) and the bond angle distribution function BADF (Ge–Ge–Ge) for the model data (lines) and the results of the RMC simulations (bars) for crystalline germanium.

Table 1
Values of mean-square displacements ($\langle u^2 \rangle$), mean-square relative displacements (σ^2) and the mean coordination shell radii $\langle R \rangle$ in crystalline germanium at 395 K for the starting model and obtained by the RMC simulation for a $4 \times 4 \times 4$ supercell.

	Starting model	RMC result
$\langle R \rangle_{1st\ shell}$ (Å)	2.45479 ± 0.00006	2.454 ± 0.003
$\langle R \rangle_{2nd\ shell}$ (Å)	4.00458 ± 0.00006	4.004 ± 0.003
$\langle R \rangle_{3rd\ shell}$ (Å)	4.69485 ± 0.00007	4.695 ± 0.002
$\sigma^2_{1st\ shell}$ (Å^2)	0.003262 ± 0.000005	0.004 ± 0.001
$\sigma^2_{2nd\ shell}$ (Å^2)	0.010716 ± 0.00001	0.0105 ± 0.0003
$\sigma^2_{3rd\ shell}$ (Å^2)	0.014804 ± 0.00001	0.013 ± 0.001
$\langle u^2 \rangle$ (Å^2)	0.0272 ± 0.0006	0.0214 ± 0.007

3.2. Influence of the cell size and simulation time

The cell size and the simulation time (number of the RMC steps) are important parameters, which can affect the results of the RMC simulation. Therefore, their optimal choice is crucial.

We have repeated our simulations also for two smaller supercells, $2 \times 2 \times 2$ (16 atoms) and $3 \times 3 \times 3$ (54 atoms), varying the number of the RMC steps between 10 000 and 80 000. The obtained results are compared in Fig. 5. The agreement between calculated and model EXAFS signals improves significantly by increasing the supercell size from $2 \times 2 \times 2$ to $3 \times 3 \times 3$. Further increase of the supercell size does not lead to notable improvement of the agreement between calculated and model EXAFS signals.

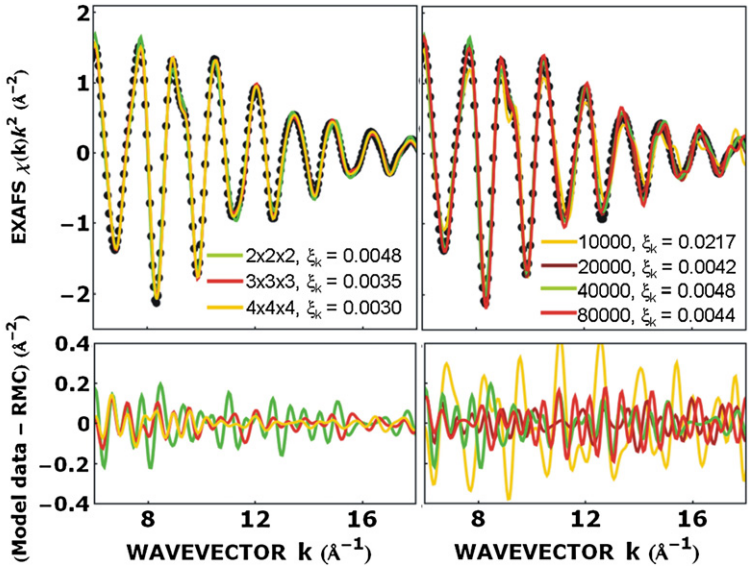

Fig. 5. (Color online.) Comparison between the model Ge K-edge EXAFS signal (dots) and the EXAFS signals, obtained from the RMC simulations of crystalline germanium using different parameters (solid lines). The corresponding differences between model signal and RMC signals are shown in the bottom panels. ξ_k is the final difference, calculated by Eq. (2). The values of the parameters are: (left panels) the length of simulation is 40 000 RMC steps and the size of the supercells are $2 \times 2 \times 2$, $3 \times 3 \times 3$, and $4 \times 4 \times 4$; (right panels) the size of the supercell is $2 \times 2 \times 2$ supercell, the lengths of simulations are 10 000, 20 000, 40 000, and 80 000 RMC steps.

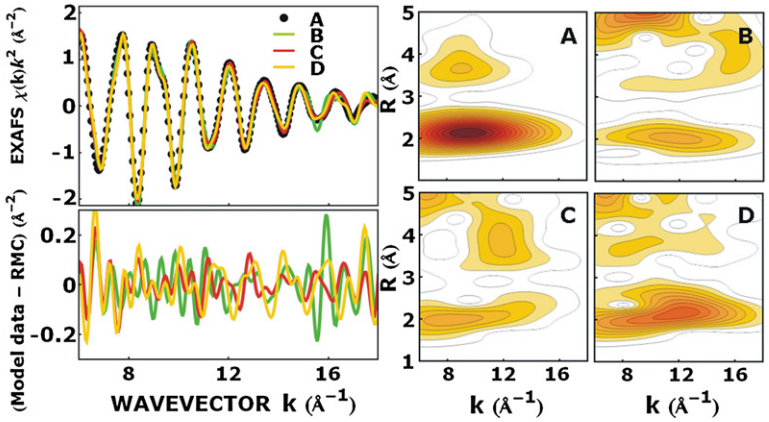

Fig. 6. (Color online.) Results of the RMC simulations with variable lattice constant for the model Ge K-edge EXAFS signal, obtained from the MD calculations of crystalline germanium. Left panel: Ge K-edge EXAFS signals for the starting MD model (A) and the result of RMC simulations with (B) the fixed lattice constant $a = 5.658$ Å, the difference $\xi_{k,R} = 0.056$; (C) the lattice constant, varying during the simulations: initial value of the lattice constant is $a = 5.608$ Å, its final value is $a = 5.652$ Å, the difference $\xi_{k,R} = 0.033$; (D) the lattice constant, varying during the simulations: initial value of lattice constant is $a = 5.708$ Å, its final value is $a = 5.679$ Å, the difference $\xi_{k,R} = 0.037$. The corresponding differences between model signal and RMC signals are shown in the bottom left panel. Right panels: (A) modulus of the wavelet transform (WT) for the model EXAFS signal; (B), (C) and (D) the WT moduli of the difference between model and calculated EXAFS signals shown in the left panel.

Therefore the increase of the supercell will not ensure the more precise determination of structure parameters. Instead, multiple RMC calculations with the same supercell but different sequences of pseudo-random numbers can be carried out to improve statistical error.

The results obtained after 20 000, 40 000 or 80 000 RMC steps are very close to each other and to the model data. However, the shorter simulation with just 10 000 RMC steps results in the EXAFS signal, which deviates strongly from the model one giving the ξ_k value about five times larger.

Finally, one can conclude that in the case of crystalline germanium, the good results can be obtained already for the size of the supercell $3 \times 3 \times 3$ and the number of the RMC steps being at least 40 000.

3.3. Determination of the lattice parameters

The RMC simulations discussed above were all performed at the fixed cell size. However, when the lattice parameters of the crystal are not known accurately enough (better than 0.01 Å), the cell size and shape should be adjusted during the RMC run. In this case, the values of the lattice constants and angles become additional degrees of freedom and can be slightly and randomly changed at each RMC step.

For cubic crystalline germanium, there is only one parameter, the lattice constant a_{Ge}, determining the cell. Therefore, it is a simple case, for which the calculations can be easily performed, and their results are shown in Fig. 6. The RMC simulation was done for $3 \times 3 \times 3$ supercell and 40 000 RMC steps. It should be noted, that the difference between the model and calculated EXAFS signals has been evaluated using the wavelet transform (Eq. (4)), since we found that the calculations in k-space were less accurate. This example shows that the use of the WT as a criterion for minimization has an advantage, even if it is more computationally heavy.

As one can see in Fig. 6, the variation of lattice constant a_{Ge} during the RMC process results in a good agreement between the

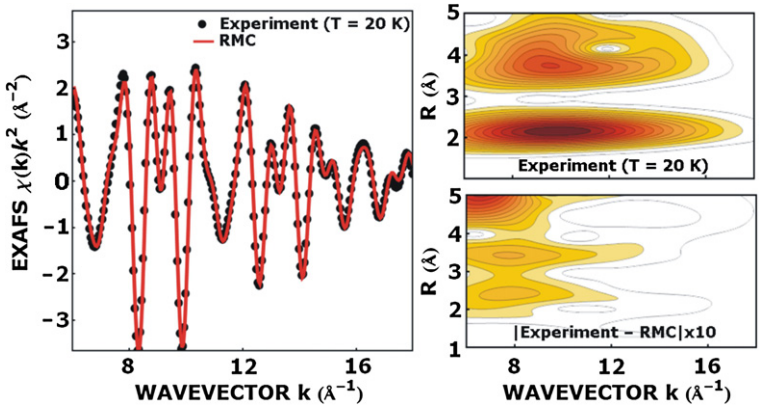

Fig. 7. (Color online.) Left panel: Experimental and calculated by the RMC method Ge K-edge EXAFS signals for crystalline germanium at $T = 20$ K. Right upper panel: WT modulus of experimental EXAFS signal. Right lower panel: modulus of the difference between WT of experimental and calculated EXAFS signals. The difference $\xi_{k,R} = 0.065$ (Eq. (4)).

model and calculated EXAFS signals. The obtained value a_{Ge} agree with the expected one within about 0.02 Å: such accuracy is sufficient for the conventional EXAFS analysis.

4. Application of the RMC-EXAFS method to experimental data

4.1. Crystalline germanium (Ge)

Next we will apply the proposed RMC scheme to the analysis of experimental Ge K-edge EXAFS in crystalline germanium [44].

While the model discussed in Section 3 is very close to the experimental EXAFS spectrum, nevertheless, there are several factors being responsible for the observed difference: (i) the already mentioned problem with the value of the lattice parameters; (ii) the influence of experimental noise; (iii) the influence of outer coordination shells; (iv) the presence of the S_0^2 factor reducing the amplitude of the EXAFS signal and having usually values in the range between 0.7 and 1.0 [49]; (v) the problem of the E_0 choice. The parameter E_0 is never known precisely and, in principle, can be even different for several measurements of the same sample due to, for example, instability of the monochromator positions during the experiment.

The first problem has been already addressed in Section 3.3. The second and third problems can be treated using proper Fourier or wavelet filtering of the experimental signal. The fourth and the fifth problems require to estimate additional parameters S_0^2 and E_0. In principle, they can be calculated in the same way as the lattice parameters during the RMC simulations. However, such approach is complicated due to strong correlations between S_0^2 and the EXAFS signal amplitude, and between E_0 and the EXAFS signal frequency. Therefore, in this work we did not refine S_0^2 and E_0 during the RMC calculations. Instead, before the simulations we carried out the conventional analysis of the EXAFS signal from the first coordination shell [56], and obtained the values of S_0^2 and E_0, which were fixed in the further RMC calculations.

For the analysis of the experimental EXAFS spectra of crystalline germanium (taken from [57]), measured in the temperature range from 20 K to 300 K, the $3 \times 3 \times 3$ supercell was constructed, and the RMC simulations were carried out for 40 000 steps. The lattice constant was fixed during the calculations at the known experimental value $a_{Ge} = 5.658$ Å [55]. The minimization was performed using the wavelet transform criterion (Eq. (4)).

The experimental Ge K-edge EXAFS spectrum, measured at 20 K, and the result of the RMC simulations are compared in Fig. 7. Note that while the theoretical EXAFS signal includes all multiple-scattering contributions in the range up to 6 Å around the absorber, their importance is not crucial in this case [43]. The

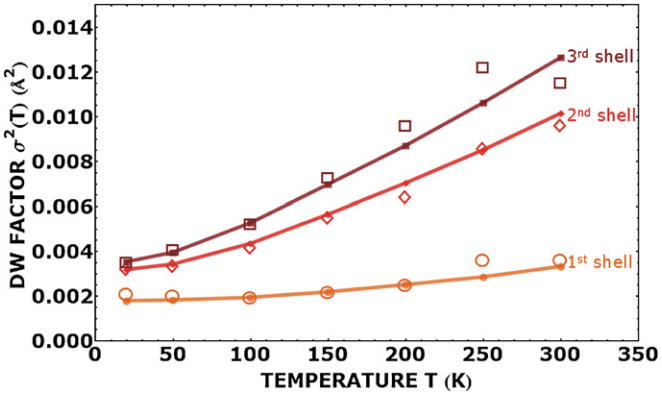

Fig. 8. (Color online.) Temperature dependence of MSRD, obtained by conventional method [57] (lines and solid symbols), and calculated using the proposed RMC scheme (open symbols) for the 1st, 2nd, and 3rd coordination shells of Ge in crystalline germanium.

temperature-dependencies of the mean-square relative displacement (MSRD) for the first, second and third coordination shells, obtained from the RMC simulations and using conventional EXAFS analysis [57], are compared in Fig. 8. The agreement between the two results is good, so one can conclude that the accuracy of the proposed method is sufficient to analyze the thermal disorder in crystalline material.

4.2. Crystalline rhenium trioxide (ReO_3)

In this section we apply the RMC method to the analysis of the Re L_3-edge EXAFS spectrum from cubic perovskite-type rhenium trioxide (space group $Pm\bar{3}m$). Temperature-dependent experimental EXAFS data were taken from [45]. As before, the $3 \times 3 \times 3$ supercell, containing 108 atoms, was used in the RMC simulations, which were carried out for 40 000 RMC steps. The lattice constant was fixed during the calculations at the experimental value $a_{ReO_3} = 3.747$ Å [58]. The minimization was performed using the wavelet transform criterion (Eq. (4)).

An example of the used supercell, the experimental Re L_3-edge EXAFS spectrum, measured at 10 K [45], and the results of the RMC simulation are shown in Fig. 9. The experimental EXAFS signal is very well reproduced by the simulation in the k-space range from 1.5 Å^{-1} to 18 Å^{-1}. It can be also seen that opposite to the case of crystalline Ge, the multiple-scattering contributions in the Re L_3-edge EXAFS spectrum of ReO_3 are very important [31,59–61], giving major contribution at large k-values. They are fully taken into account in our RMC simulations.

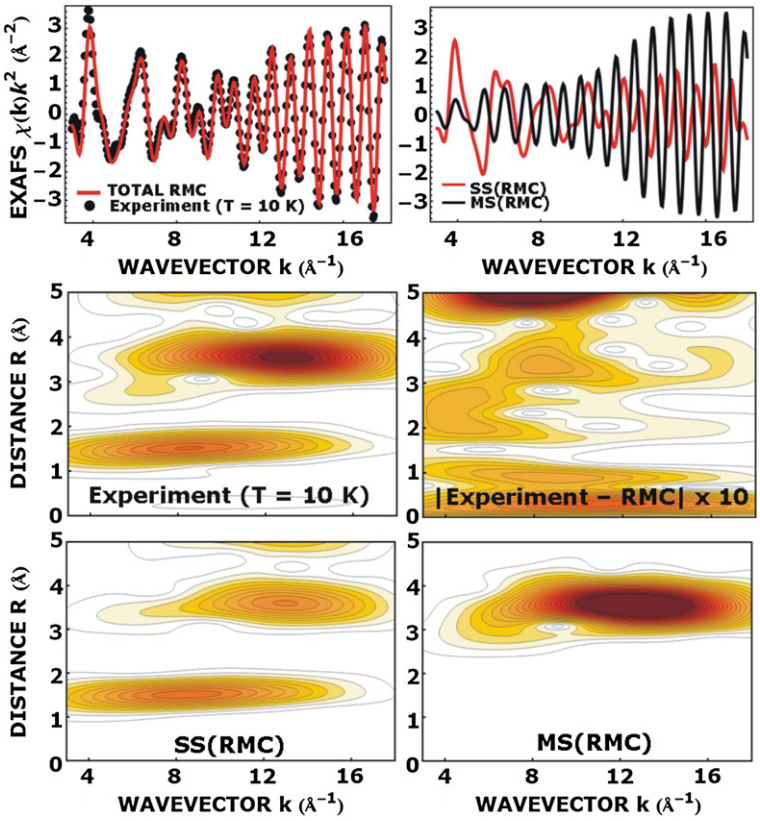

Fig. 9. (Color online.) Upper panels: experimental and calculated by the RMC method Re L_3-edge EXAFS signals $\chi(k)k^2$ at $T = 10$ K. Single-scattering (SS) and multiple scattering (MS) contributions are shown separately. Middle panels: WT moduli of experimental EXAFS signal and of the difference between calculated and experimental EXAFS signals. Lower panels: WT moduli of calculated SS and MS contributions into the total EXAFS signal. The difference $\xi_{k,R} = 0.107$ (Eq. (4)).

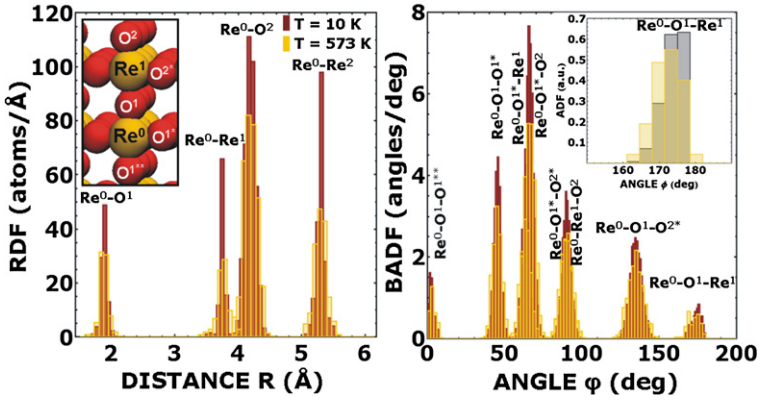

Fig. 10. (Color online.) Calculated radial distribution functions RDF (Re–O) and RDF (Re–Re) and the bond angle distribution functions BADF (Re–O–O), BADF (Re–Re–O), and BADF (Re–O–Re) at $T = 10$ K (red bars) and $T = 573$ K (yellow bars) for ReO_3. The inset shows the distribution of the Re–O–Re angle at $T = 573$ K: results of RMC calculations (yellow bars) and results of the MD simulations [63].

In Fig. 10 the radial (RDF) and bond angle (BADF) distribution functions, calculated from the final atomic configuration, are shown for low ($T = 10$ K) and high ($T = 573$ K) temperatures. As one expects, the peaks of the radial distribution function become broadened upon increasing temperature. An interesting feature of the BADF is the peak at 170°–180°, corresponding to the angle Re^0–O^1–Re^1 (here Re^0 is the absorbing atom, O^1 and Re^1 are atoms in the first and second coordination shells, respectively). The BADF peak has asymmetric shape, and its maximum is not located at 180°, as one could expect for the linear Re–O–Re chain in cubic ReO_3, but is shifted to lower value of ∼ 172°. This effect is caused by the large thermal vibrations of oxygen atoms in the directions orthogonal to the Re–Re bonds [59,62,63].

5. Conclusions

In this work we propose the improved Reverse Monte Carlo (RMC) scheme for the analysis of the EXAFS spectra. In our approach, the difference between theoretical and experiment EXAFS signals is minimized during the RMC simulation simultaneously in k and R spaces by using the modified Morlet continuous wavelet transform of the EXAFS signal (Eq. (4)) [40]. Besides, to improve convergence during the simulation, we use slowly reducing "temperature" parameter (Eq. (6)) in the Metropolis algorithm (the so-called simulated annealing method [41]).

The use of the method is demonstrated on the example of the EXAFS spectra analysis for the model system and experimental

data for crystalline germanium and rhenium trioxide. It is shown that the method allows one to reconstruct the 3D atomic structure of the compound taking into account the thermal disorder and to obtain the distributions of distances and bond angles describing the local structure around the absorber. Also the uncorrelated (MSD) and correlated (MSRD) thermal vibration amplitudes can be recovered with reasonable accuracy. The obtained results for Ge and ReO_3 are in good agreement with that previously found by conventional EXAFS analysis and molecular dynamics simulations.

Acknowledgements

This work was supported by ESF Projects Nos. 2009/0202/1DP/1.1.1.2.0/09/APIA/VIAA/141, 2009/0216/1DP/1.1.1.2.0/09/APIA/VIAA/044 and Latvian Government Research Grant No. 09.1518.

References

[1] R. McGreevy, L. Pusztai, Mol. Simul. 1 (1988) 359.
[2] G. Opletal, T. Petersen, B. O'Malley, I. Snook, D.G. McCulloch, N.A. Marks, I. Yarovsky, Mol. Simul. 28 (2002) 927.
[3] R.L. McGreevy, J. Phys.: Condens. Matter 13 (2001) R877.
[4] M.T. Dove, M.G. Tucker, S.A. Wells, D.A. Keen, EMU Notes Mineral. 4 (2002) 59.
[5] R.L. McGreevy, P. Zetterstrom, J. Non-Cryst. Solids 293–295 (2001) 297.
[6] A. Mellergård, R.L. McGreevy, S.G. Eriksson, J. Phys.: Condens. Matter 12 (2000) 4975.
[7] M.G. Tucker, M.T. Dove, D.A. Keen, J. Appl. Cryst. 34 (2001) 630.
[8] M. Winterer, R. Delaplane, R. McGreevy, J. Appl. Cryst. 35 (2002) 434.
[9] D.A. Keen, M.G. Tucker, M.T. Dove, J. Phys.: Condens. Matter 17 (2005) S15.
[10] M.G. Tucker, D.A. Keen, M.T. Dove, A.L. Goodwin, Q. Hui, J. Phys.: Condens. Matter 19 (2007) 335218.
[11] P. Zetterström, S. Urbonaite, F. Lindberg, R.G. Delaplane, J. Leis, G. Svensson, J. Phys.: Condens. Matter 17 (2005) 3509.
[12] N. Bedford, C. Dablemont, G. Viau, P. Chupas, V. Petkov, J. Phys. Chem. C 111 (2007) 18214.
[13] V. Petkov, N. Bedford, M.R. Knecht, M.G. Weir, R.M. Crooks, W. Tang, G. Henkelman, A. Frenkel, J. Phys. Chem. C 112 (2008) 8907.
[14] N.M. Bedford, Solid State Commun. 150 (2010) 1505.
[15] S.J. Gurman, R.L. McGreevy, J. Phys.: Condens. Matter 2 (1990) 9463.
[16] J.D. Wicks, R.L. McGreevy, J. Non-Cryst. Solids 192–193 (1995) 23.
[17] M. Winterer, J. Appl. Phys. 88 (2000) 5635.
[18] A. Di Cicco, A. Trapananti, S. Faggioni, A. Filipponi, Phys. Rev. Lett. 91 (2003) 135505.
[19] A. Di Cicco, A. Trapananti, J. Phys.: Condens. Matter 17 (2005) S135.
[20] G. Evrard, L. Pusztai, J. Phys.: Condens. Matter 17 (2005) S1.
[21] O. Gereben, P. Jóvári, L. Temleitner, L. Pusztai, J. Opt. Adv. Mater. 9 (2007) 3021.
[22] W.K. Luo, E. Ma, J. Non-Cryst. Solids 354 (2008) 945.
[23] V. Krayzman, I. Levin, M.G. Tucker, J. Appl. Cryst. 41 (2008) 705.
[24] V. Krayzman, I. Levin, J.C. Woicik, Th. Proffen, T.A. Vanderah, M.G. Tucker, J. Appl. Cryst. 42 (2009) 867.
[25] M. Leetmaa, K.T. Wikfeldt, L.G.M. Pettersson, J. Phys.: Condens. Matter 22 (2010) 135001.
[26] V. Krayzman, I. Levin, J. Phys.: Condens. Matter 22 (2010) 404201.
[27] C.A. Ashley, S. Doniach, Phys. Rev. B 11 (1975) 1279.
[28] P.A. Lee, J.B. Pendry, Phys. Rev. B 11 (1975) 2795.
[29] N. Alberding, E.D. Crozier, R. Ingals, B. Houser, J. Phys. (Paris) 47 (1986) 681.
[30] R.V. Vedrinskii, L.A. Bugaev, I.G. Levin, Phys. Status Solidi (b) 150 (1988) 307.
[31] A. Kuzmin, J. Purans, M. Benfatto, C.R. Natoli, Phys. Rev. B 47 (1993) 2480.
[32] A. Kuzmin, J. Purans, J. Phys.: Condens. Matter 5 (1993) 9423.
[33] A. Kuzmin, J. Purans, J. Phys.: Condens. Matter 5 (1993) 267.
[34] A. Kuzmin, Ph. Parent, J. Phys.: Condens. Matter 6 (1994) 4395.
[35] J.B. Goodenough, Structure Bonding 98 (2001) 1.
[36] A. Kuzmin, R. Grisenti, Philos. Mag. B 70 (1994) 1161.
[37] J. Garcia, A. Bianconi, M. Benfatto, C.R. Natoli, J. Phys. 47 (1986) C8-49.
[38] A. Kuzmin, S. Obst, J. Purans, J. Phys.: Condens. Matter 9 (1997) 10069.
[39] http://www.rmcprofile.org/.
[40] J. Timoshenko, A. Kuzmin, Comput. Phys. Comm. 180 (2009) 920.
[41] S. Kirkpatrick, C.D. Gelatt, M.P. Vecchi, Science 220 (1983) 671.
[42] A. Kuzmin, Latvian J. Phys. Tech. Sci. 2 (2006) 7.
[43] J. Timoshenko, A. Kuzmin, J. Purans, Centr. Eur. J. Phys. 9 (2011) 710.
[44] J. Purans, N.D. Afify, G. Dalba, R. Grisenti, S.D. Panfilis, A. Kuzmin, V.I. Ozhogin, F. Rocca, A. Sanson, S.I. Tiutiunnikov, P. Fornasini, Phys. Rev. Lett. 100 (2008) 055901.
[45] J. Purans, G. Dalba, P. Fornasini, A. Kuzmin, S.D. Panfilis, F. Rocca, AIP Conf. Proc. 882 (2007) 422.
[46] A.L. Ankudinov, B. Ravel, J.J. Rehr, S.D. Conradson, Phys. Rev. B 58 (1998) 7565.
[47] A. Filipponi, A. Di Cicco, C.R. Natoli, Phys. Rev. B 52 (1995) 15122.
[48] J.J. Rehr, J.J. Kas, M.P. Prange, A.P. Sorini, Y. Takimoto, F. Vila, C. R. Phys. 10 (2009) 548.
[49] J.J. Rehr, R.C. Albers, Rev. Modern Phys. 72 (2000) 621.
[50] M. Munoz, P. Argoul, F. Farges, Am. Mineral. 88 (2003) 694.
[51] M. Matsumoto, T. Nishimura, ACM Trans. Model. Comput. Simul. 8 (1998) 3.
[52] N. Metropolis, A.W. Rosenbluth, M.N. Rosenbluth, A.H. Teller, E. Teller, J. Chem. Phys. 21 (1953) 1087.
[53] D. Bertsimas, J. Tsitsiklis, Statist. Sci. 8 (1993) 10.
[54] B. Hajek, Math. Oper. Res. 13 (1988) 311.
[55] A. Smakula, J. Kalnajs, V. Sils, Phys. Rev. 99 (1955) 1747.
[56] A. Kuzmin, Physica B 208–209 (1995) 175.
[57] J. Purans, J. Timoshenko, A. Kuzmin, G. Dalba, P. Fornasini, R. Grisenti, N.D. Afify, F. Rocca, S.D. Panfilis, I. Ozhogin, S.I. Tiutiunnikov, J. Phys.: Conf. Ser. 190 (2009) 012063.
[58] T. Chatterji, P.F. Henry, R. Mittal, S.L. Chaplot, Phys. Rev. B 78 (2008) 134105.
[59] B. Houser, R. Ingalls, J.J. Rehr, Physica B 208–209 (1995) 323.
[60] G. Dalba, P. Fornasini, A. Kuzmin, J. Purans, F. Rocca, J. Phys.: Condens. Matter 7 (1995) 1199.
[61] A. Kuzmin, J. Purans, G. Dalba, P. Fornasini, F. Rocca, J. Phys.: Condens. Matter 8 (1996) 9083.
[62] B. Houser, R. Ingalls, Phys. Rev. B 61 (2000) 6515.
[63] A. Kalinko, R.A. Evarestov, A. Kuzmin, J. Purans, J. Phys.: Conf. Ser. 190 (2009) 012080.